

A combined analysis of all data on ν and $\bar{\nu}$ induced single-charm production

G. De Lellis¹⁾, A. Marotta¹⁾ and P. Migliozzi²⁾

1) Università Federico II and INFN, Napoli, Italy

2) INFN, Napoli, Italy

Abstract

Neutrino and anti-neutrino induced single-charm production are particularly interesting to study the strange-quark parton distribution function and the threshold effect in the cross-section, associated with the heavy quark production. Over the past 30 years, many experiments have carried out these studies with complementary techniques: calorimetry, bubble chambers and nuclear emulsions.

In this paper, we review these data and combine them statistically to extract a world averaged single-charm production cross-section for both neutrino and anti-neutrino.

1 Introduction

Neutrino and anti-neutrino induced charm-production is interesting because it can be used to isolate the strange-quark parton distribution function and to study the transition to heavy quarks. In particular, the understanding of the threshold behavior associated with the charm-production is critical for the extraction of $\sin^2 \theta_W$ from neutrino deep-inelastic data. Furthermore, a better understanding of the inclusive charm-production cross-section is crucial for the background determination of future experiments aiming at the study of neutrino oscillations.

This paper is organized as follows: in Section 2 we briefly discuss how charm-production can be studied by looking at the so-called di-lepton events and review all available di-lepton data. In Section 3 the inclusive charm search by using nuclear emulsions is discussed together with the available data. In Section 4 the di-lepton and emulsion data are combined to compute a world averaged inclusive charm-production cross-section.

2 Charm-production studies with di-leptons

2.1 Experimental issues

Many experiments have studied neutrino and anti-neutrino charm-production by looking at the presence of two oppositely charged leptons in the final state. This technique was firstly used in 1974 [1] when the neutrino induced charm-production was discovered.

In the case of neutrino scattering, the underlying process is a neutrino charged-current (CC) interaction with an s or d quark, producing a charm-quark that fragments into a charmed hadron. The charmed hadron may decay semi-leptonically producing opposite sign di-leptons through the process:

$$\begin{aligned} \nu_\mu + N &\longrightarrow \mu^- + c + X \\ &\hookrightarrow s + l^+ + \nu_l \end{aligned} \tag{1}$$

Analogously an anti-neutrino can interact with a \bar{s} or \bar{d} anti-quark, producing a charm anti-quark that fragments into a charmed hadron, again leading to a final state with two oppositely charged leptons.

Since 1974, several experiments ([2] to [11]) have used this technique to study charm-production. They can be separated in two classes: calorimetric and bubble chamber experiments, exploiting the muonic and electronic decay of the charmed hadron, respectively.

Calorimetric experiments are characterized by a massive iron target and a muon spectrometer to identify the muon and measure its charge. For these experiments pion and kaon decays constitute the main background. The high density of the target calorimeter minimizes this background due to the short interaction length of the detector. A further background reduction is obtained

by requiring a minimum momentum, typically $p_\mu > 5$ GeV, for the less energetic muon. The drawback of such a selection is that these experiments are not able to search for charm-production at relatively low neutrino energies. For a typical calorimetric experiment it is not possible to investigate energy regions below 15 GeV, where the slow-rescaling threshold effect is more important.

The main characteristic of a bubble chamber filled with a mixture of heavy liquids (Ne-H₂, freon-propane) is its high efficiency in identifying electrons. Therefore, they searched for charm-production by looking at $\mu^- e^+$ events. In these experiments, the low threshold, $p_{e^+} > 0.3$ GeV, combined with high statistics for $E_\nu < 30$ GeV, gives good sensitivity to the slow-rescaling threshold behaviour. The main background sources for these searches are π^0 Dalitz decays and $\bar{\nu}_e$ CC interactions.

2.2 Di-lepton data sample and selection criteria

Table 1 summarises the available (anti-)neutrino di-lepton data samples.

The data selection is similar for all calorimetric experiments, although the kinematical cuts can be slightly different. In the following we describe qualitatively the data selection flow:

- the event must occur in coincidence with the beam and fire the penetration trigger (CC interaction trigger);
- to ensure both the longitudinal and transverse containment of the hadronic shower a fiducial cut is applied;
- both muons have to be well reconstructed, with the closest approach between them being less than a certain distance (typically $\mathcal{O}(10$ cm)). This cut allows to reject overlays of two CC events as well as obvious muons from the decay of shower hadrons.

The di-lepton events are categorised as originating from an incident neutrino or anti-neutrino by assuming that the primary muon (the muon produced at the leptonic vertex) is the one with the largest transverse momentum with respect to the beam direction.

For each event, the reconstructed muon parameters at the vertex (\vec{p}_i , E_i , $\vec{r}_i = \vec{p}_i / |p_i|$, $i = 1, 2$) and the shower energy E_{had} , are used to compute the following kinematical variables:

- $E_{vis}^\nu = E_1 + E_2 + E_{had}$, the visible neutrino energy;
- $Q_{vis}^2 = 2E_{vis}^\nu(E_1 - \vec{p}_1 \cdot \vec{i}) - m_\mu^2$, the visible negative four-momentum transfer squared, where \vec{p}_1 is the leading muon 3-momentum and \vec{i} represents a unit vector parallel to the beam direction;
- $\nu_{vis} = E_2 + E_{had}$, the visible energy transferred to the hadronic system;
- $x_{vis} = Q_{vis}^2 / 2M\nu_{vis}$, the visible Bjorken x ;

Experiment	Technique	l^-l^+ sample	l^+l^- sample
CDHS [2]	Calorimetry	9922	2123
LBL Coll. [3]	Bubble Chamber	$\mathcal{O}(50)$	—
CBNL Coll. [4]	Bubble Chamber	$\mathcal{O}(100)$	—
NOMAD [5]	Calorimetry	2714 ± 227	115^{+38}_{-41}
CCFR [6]	Calorimetry	4247 ± 90	944 ± 34
Gargamelle I [7]	Bubble Chamber	62 ± 10	—
Gargamelle II [8]	Bubble Chamber	$\mathcal{O}(50)$	—
E53A+E53B [9]	Bubble Chamber	602 ± 208	—
Foudas et al. [10]	Bubble Chamber	1460.4 ± 42.1	223.5 ± 5.0
E616+E701 [11]	Calorimetry	852 ± 77	68 ± 16

Table 1: Available (anti-)neutrino di-lepton data samples. The samples are background subtracted.

- $y_{vis} = \nu_{vis}/E_{vis}^\nu$, the visible Bjorken y .

In addition to the topological cuts listed above, a set of kinematical cuts is also applied. Both muons are required to have an energy greater than 4-10 GeV, primarily to reduce the meson decay background. The visible hadronic energy is required to be more than 5-20 GeV to ensure a good hadronic energy reconstruction.

The bubble chamber experimental search for charm-production relies upon its high efficiency in identifying electrons. Therefore, in order to identify μ^-e^+ dilepton candidates, the film is scanned for all events with an e^+ coming from the vertex with a momentum greater than 300 MeV. To be identified as an e^+ , the track is required to exhibit at least two characteristics of positrons in heavy liquid. The signatures are:

- bremsstrahlung with a $\gamma \rightarrow e^+e^-$ conversion;
- spiralisation;
- production of a δ ray with energy comparable to the primary track;
- annihilation with two $\gamma \rightarrow e^+e^-$ conversions.

After being scanned, measured and reconstructed, each event containing an e^+ track is carefully analyzed, a fiducial volume cut applied and the search for at least one leaving negative (L^-) track performed. The highest momentum L^- track in each event is interpreted as a muon leaving the chamber. Under this assumption, a kinematical analysis is applied in order to select genuine $\nu_\mu CC$ interactions.

2.3 The average di-lepton charm-production cross-section

In order to combine all di-lepton data (see Tables 2, 3 and 4) it is necessary to make a bin by bin weighted average. Since different experiments have different

CDHS			LBL		
E_ν (GeV)	$\langle E_\nu \rangle$ (GeV)	$\sigma_{l-l^+}/\sigma_{CC}$ (%)	E_ν (GeV)	$\langle E_\nu \rangle$ (GeV)	$\sigma_{l-l^+}/\sigma_{CC}$ (%)
30-40	35	0.19 ± 0.08	0-30	15	$0.21^{+0.65}_{-0.11}$
40-60	50	0.40 ± 0.11	30-60	45	0.71 ± 0.19
60-80	70	0.53 ± 0.10	60-100	80	0.71 ± 0.19
80-100	90	0.60 ± 0.11	100-170	135	0.78 ± 0.24
100-120	110	0.61 ± 0.11	170-280	225	0.95 ± 0.36
120-140	130	0.69 ± 0.13	—	—	—
140-160	150	0.68 ± 0.11	—	—	—
160-180	170	0.69 ± 0.13	—	—	—
180-200	190	0.73 ± 0.13	—	—	—
200-240	220	0.76 ± 0.13	—	—	—
CBNL			NOMAD		
E_ν (GeV)	$\langle E_\nu \rangle$ (GeV)	$\sigma_{l-l^+}/\sigma_{CC}$ (%)	E_ν (GeV)	$\langle E_\nu \rangle$ (GeV)	$\sigma_{l-l^+}/\sigma_{CC}$ (%)
0-15	7.5	0.19 ± 0.07	0-20	10	0.23 ± 0.11
15-30	22.5	0.53 ± 0.09	20-40	30	0.36 ± 0.11
30-60	45	$0.55^{+0.10}_{-0.08}$	40-70	55	0.47 ± 0.14
60-100	80	$0.82^{+0.26}_{-0.24}$	70-100	85	0.61 ± 0.15
100-150	120	$0.95^{+0.29}_{-0.31}$	100-200	135	0.68 ± 0.17
—	—	—	200-300	235	0.53 ± 0.39
CCFR			Foudas et al.		
E_ν (GeV)	$\langle E_\nu \rangle$ (GeV)	$\sigma_{l-l^+}/\sigma_{CC}$ (%)	E_ν (GeV)	$\langle E_\nu \rangle$ (GeV)	$\sigma_{l-l^+}/\sigma_{CC}$ (%)
—	40	0.54 ± 0.05	10-70	50	0.63 ± 0.11
—	70	0.64 ± 0.04	70-100	80	0.60 ± 0.07
—	90	0.66 ± 0.04	100-150	120	$0.75^{+0.07}_{-0.04}$
—	110	0.65 ± 0.03	150-200	170	0.77 ± 0.04
—	140	0.77 ± 0.04	200-250	220	0.84 ± 0.07
—	180	0.84 ± 0.03	250-300	270	$0.86^{+0.09}_{-0.07}$
—	220	0.86 ± 0.03	300-350	320	$0.99^{+0.09}_{-0.11}$
—	270	0.92 ± 0.03	350-400	370	$0.97^{+0.15}_{-0.13}$
—	330	0.89 ± 0.05	400-600	450	1.10 ± 0.18
—	450	0.95 ± 0.05	—	—	—

Table 2: Di-lepton neutrino cross-section, normalized to the CC cross-section, as a function of the neutrino energy, for some ([2] to [6], [10]) electronic detector experiments.

Gargamelle I			Gargamelle II		
E_ν (GeV)	$\langle E_\nu \rangle$ (GeV)	$\sigma_{l-l^+}/\sigma_{CC}$ (%)	E_ν (GeV)	$\langle E_\nu \rangle$ (GeV)	$\sigma_{l-l^+}/\sigma_{CC}$ (%)
15-35	—	0.65 ± 0.23	10-30	20	$0.28^{+0.14}_{-0.16}$
35-75	—	0.69 ± 0.22	30-70	50	0.43 ± 0.12
75-300	—	0.89 ± 0.23	70-150	110	$0.65^{+0.32}_{-0.30}$
E53A+E53B			E616+E701		
E_ν (GeV)	$\langle E_\nu \rangle$ (GeV)	$\sigma_{l-l^+}/\sigma_{CC}$ (%)	E_ν (GeV)	$\langle E_\nu \rangle$ (GeV)	$\sigma_{l-l^+}/\sigma_{CC}$ (%)
0-25	12.5	0.20 ± 0.04	30-100	70	0.48 ± 0.06
25-50	37.5	0.51 ± 0.08	100-180	150	0.81 ± 0.10
50-100	75	0.60 ± 0.10	180-230	200	0.90 ± 0.10
100-200	150	0.60 ± 0.15	—	—	—

Table 3: Di-lepton neutrino cross-section, normalized to the CC cross-section, as a function of the neutrino energy, for some ([7] to [9] and [11]) electronic detector experiments.

CDHS			CCFR		
E_ν (GeV)	$\langle E_\nu \rangle$ (GeV)	$\sigma_{l+l^-}/\sigma_{CC}$ (%)	E_ν (GeV)	$\langle E_\nu \rangle$ (GeV)	$\sigma_{l+l^-}/\sigma_{CC}$ (%)
30-40	35	0.30 ± 0.11	—	40	0.58 ± 0.09
40-60	50	0.53 ± 0.12	—	70	0.72 ± 0.07
60-80	70	0.71 ± 0.15	—	90	0.73 ± 0.05
80-100	90	0.78 ± 0.17	—	110	0.95 ± 0.08
100-120	110	0.78 ± 0.17	—	140	0.88 ± 0.07
120-140	130	0.83 ± 0.18	—	180	1.05 ± 0.08
140-160	150	0.86 ± 0.19	—	220	1.08 ± 0.11
—	—	—	—	270	0.97 ± 0.11
—	—	—	—	330	1.30 ± 0.22
—	—	—	—	450	0.97 ± 0.27
E616+E701			Foudas et al.		
E_ν (GeV) (GeV)	$\langle E_\nu \rangle$ (GeV)	$\sigma_{l+l^-}/\sigma_{CC}$ (%)	E_ν (GeV)	$\langle E_\nu \rangle$ (GeV)	$\sigma_{l+l^-}/\sigma_{CC}$ (%)
30-100	60	0.38 ± 0.13	12-65	50	0.63 ± 0.15
100-230	150	0.85 ± 0.27	65-95	80	0.84 ± 0.15
—	—	—	95-145	120	0.72 ± 0.12
—	—	—	145-195	170	0.90 ± 0.12
—	—	—	195-290	230	0.84 ± 0.12
—	—	—	290-600	350	1.25 ± 0.30

Table 4: Di-lepton anti-neutrino cross-section, normalized to the CC cross-section, as a function of the neutrino energy, for the electronic detector experiments.

binning, we have to define weighting criteria to combine them all into an unique re-binning of the neutrino energy range: 0-600 GeV divided into 60 bins. The data-point in the j -th bin $((X_j, Y_j), j \in \{1, \dots, 60\})$ is calculated once we have assigned a given weight to the data-point (x_{ik}, y_{ik}) of the k -th bin of the i -th experiments, here-after called source bin, according to the following criteria:

- the wider the source-bin (Δx_{ik}) , the smaller the weight;
- the wider the error (Δy_{ik}) , the smaller the weight;
- the larger the fraction f_{ijk} of the j -th bin covered by the source bin, the larger the weight.

It is then possible to make a bin by bin weighted average of the data-points by using the following formulae:

- data-point weight

$$\omega_{ijk} = \left(\frac{f_{ijk}}{\Delta y_{ik} \cdot \Delta x_{ik}} \right)^2$$

- data-point average

$$\bar{Y}_j = \frac{\sum_{i,k} y_{ik} \cdot \omega_{ijk}}{\sum_{i,k} \omega_{ijk}}$$

- data-point error

$$\Delta \bar{Y}_j = \frac{\sqrt{\sum_{i,k} \Delta y_{ik}^2 \cdot \omega_{ijk}^2}}{\sum_{i,k} \omega_{ijk}}$$

Since CCFR data do not report the energy bins, it is not possible to combine them with the others at this stage of the analysis.

Once the average has been computed, the CCFR data are combined with the other ones in the following way: each CCFR data-point is assigned to the bin containing its x-value, then a standard weighted average between the CCFR data-point and the previous combined data is calculated. In this case, the inverse of the Δy squared is used as weight.

The average di-lepton single-charm production cross-sections for both ν and $\bar{\nu}$ are shown in Tables 5 and 6, and Figs. 1 and 2, respectively.

3 Charm-production studies with nuclear emulsions

3.1 Experimental issues

So far only two experiments, E531 [12] and CHORUS [13], have searched for inclusive charm-production through the direct identification of charm decays in the emulsions. The main advantage of these experiments is that, being the

Energy (GeV)	$\sigma_{l-l^+}/\sigma_{CC}$ (%)	Energy (GeV)	$\sigma_{l-l^+}/\sigma_{CC}$ (%)	Energy (GeV)	$\sigma_{l-l^+}/\sigma_{CC}$ (%)
5	$0.20^{+0.05}_{-0.03}$	145	0.76 ± 0.03	285	0.86 ± 0.08
15	$0.24^{+0.04}_{-0.02}$	155	0.73 ± 0.05	295	0.86 ± 0.08
25	$0.42^{+0.05}_{-0.04}$	165	0.74 ± 0.05	350	0.92 ± 0.04
35	0.29 ± 0.06	175	0.74 ± 0.05	450	0.96 ± 0.05
45	0.51 ± 0.03	185	0.82 ± 0.03	550	1.10 ± 0.18
55	0.49 ± 0.05	195	0.77 ± 0.05		
65	0.53 ± 0.05	205	0.84 ± 0.05		
75	0.61 ± 0.03	215	0.84 ± 0.05		
85	0.60 ± 0.05	225	0.85 ± 0.03		
95	0.64 ± 0.03	235	0.81 ± 0.06		
105	0.66 ± 0.07	245	0.84 ± 0.07		
115	0.65 ± 0.03	255	0.86 ± 0.08		
125	0.72 ± 0.08	265	0.86 ± 0.08		
135	0.72 ± 0.08	275	0.91 ± 0.03		

Table 5: Average neutrino di-lepton cross-section, normalized to CC cross-section, as a function of the neutrino energy.

Energy (GeV)	$\sigma_{l+l^-}/\sigma_{CC}$ (%)	Energy (GeV)	$\sigma_{l+l^-}/\sigma_{CC}$ (%)	Energy (GeV)	$\sigma_{l+l^-}/\sigma_{CC}$ (%)
5	—	145	0.85 ± 0.16	285	0.84 ± 0.12
15	0.63 ± 0.15	155	0.87 ± 0.14	295	1.25 ± 0.30
25	0.63 ± 0.15	165	0.90 ± 0.12	350	1.28 ± 0.18
35	0.47 ± 0.07	175	1.00 ± 0.07	450	1.10 ± 0.20
45	0.53 ± 0.10	185	0.90 ± 0.12	550	1.25 ± 0.30
55	0.53 ± 0.10	195	0.88 ± 0.09		
65	0.71 ± 0.06	205	0.84 ± 0.11		
75	0.72 ± 0.11	215	0.84 ± 0.11		
85	0.74 ± 0.05	225	0.96 ± 0.08		
95	0.74 ± 0.13	235	0.84 ± 0.11		
105	0.90 ± 0.07	245	0.84 ± 0.12		
115	0.77 ± 0.13	255	0.84 ± 0.12		
125	0.80 ± 0.14	265	0.91 ± 0.08		
135	0.86 ± 0.06	275	0.84 ± 0.12		

Table 6: Average anti-neutrino di-lepton cross-section, normalized to CC cross-section, as a function of the neutrino energy.

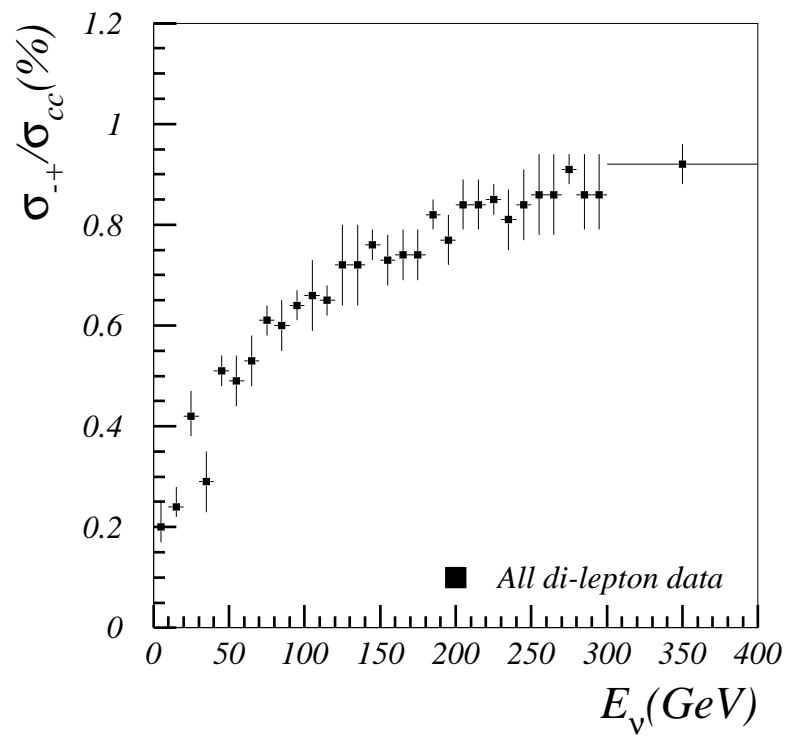


Figure 1: Average neutrino di-lepton cross-section, normalized to CC cross-section, as a function of the neutrino energy

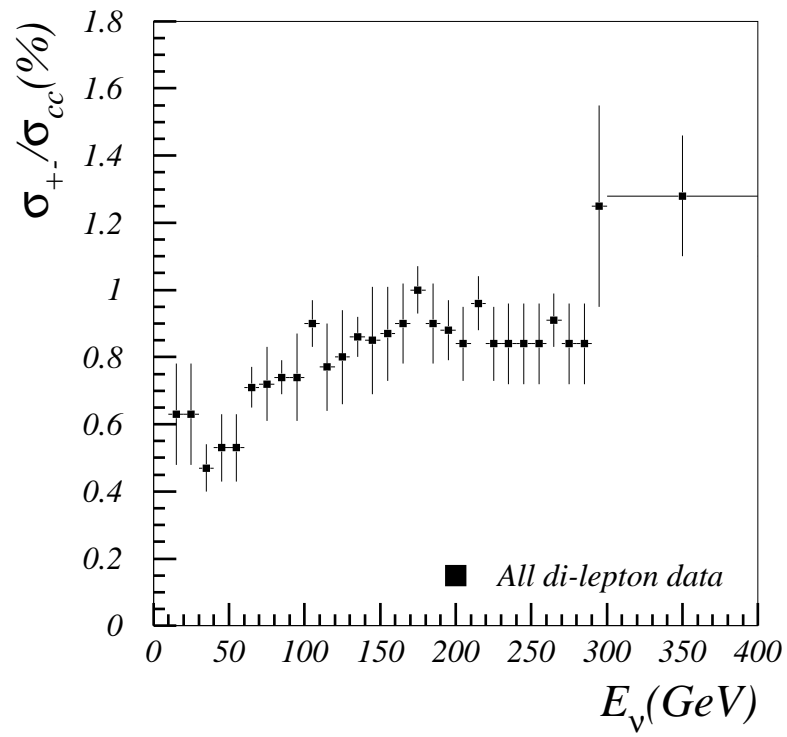


Figure 2: Average anti-neutrino di-lepton cross-section, normalized to CC cross-section, as a function of the neutrino energy.

charmed particle identified through its decay, very loose kinematical cuts are applied. This translates into a very good sensitivity to the slow-rescaling threshold behavior and consequently to the charm-quark mass.

These experiments have a hybrid design. Electronic detectors locate the regions in emulsions where the neutrino interactions occur and contribute to the reconstruction of the event kinematics. Emulsions are used as active targets. They have the appropriate position resolution (less than $1 \mu\text{m}$) and granularity to detect short-lived particles through the visual observation of their decays. The main background for D^0 detection in emulsion comes from K^0 and Λ decays, and neutron, K^0 and Λ interactions without any visible nuclear break-up at the interaction point. For charged charmed-hadrons the main backgrounds are π and K decays in flight, and the *white kink* (hadron interaction without any visible nuclear break-up) on any charged non-charmed hadron. Both the processes can be easily ruled out by applying a cut on the transverse momentum at the decay vertex ($p_T > 250 \text{ MeV}$). The contribution to the background of these processes is of the order of $10^{-4}/CC$.

3.2 Emulsion data sample and selection criteria

Although in the last years the automatic scanning of the nuclear emulsions had an impressive development, the event search principle used in the former hybrid experiment E531 is still valid for present experiments. Once the neutrino interaction is successfully reconstructed, tracks are searched for in the downstream end of the emulsion target by using the slopes and coordinates as predicted by the electronic detectors. If the predicted track is found in the most downstream emulsion sheet, it is then followed through the emulsion module up to the neutrino interaction vertex.

Once a neutrino interaction is found, an attempt is made to find possible charmed-particle decays. In the former E531 experiment semi-automatic systems were used, thus limiting the number of interactions to be studied. Nowadays, very powerful automatic systems are available allowing for a larger statistics to be searched for.

The final E531 data sample consists of 3855 neutrino interactions among which 122 charmed-particle decays are found [12]. The estimated background is 0.2 and 3.6 events for neutral and charged charmed-particle decays, respectively.

Using the weighted number of events, the relative charmed-particle production rate is: $\sigma(\nu_\mu N \rightarrow c\mu^- X)/\sigma(\nu_\mu N \rightarrow \mu^- X) = 4.9^{+0.7}_{-0.6}\%$. Table 7 shows the energy dependence of this cross-section. The analysis of the CHORUS data is still under way.

4 The world average charm-production cross-section

E_ν (GeV)	$\langle E_\nu \rangle$ (GeV)	σ_C/σ_{CC} (%)
0-10	5	$0.7^{+1.1}_{-0.6}$
10-30	20	3.6 ± 0.9
30-60	45	4.9 ± 1.1
60-150	105	10.1 ± 2.5

Table 7: Inclusive neutrino charm-production cross-section, normalized to the CC cross-section, as a function of the neutrino energy.

4.1 From the di-lepton to the total charm-production cross-section

As discussed in Section 2, calorimetric and bubble chamber experiments cannot detect directly the charmed hadrons; instead only the lepton from semi-leptonic charm decay is measured. Without going into the details, we remind that the charmed hadron (C) cross-section can be connected to the charmed quark (c) cross-section via fragmentation functions, assuming factorization [14]:

$$\begin{aligned}
\frac{d\sigma(\nu N \rightarrow \mu^- CX)}{dx dy dz dp_T^2} &= \frac{d\sigma(\nu N \rightarrow \mu^- cX)}{dx dy} \times \sum_h f_h \times D_c^h(z, p_T^2) \\
\frac{d\sigma(\bar{\nu} N \rightarrow \mu^+ \bar{C}X)}{dx dy dz dp_T^2} &= \frac{d\sigma(\bar{\nu} N \rightarrow \mu^+ \bar{c}X)}{dx dy} \times \sum_h \bar{f}_h \times \bar{D}_c^h(z, p_T^2) \quad (2)
\end{aligned}$$

Here, $D_c^h(z, p_T^2)$ is the probability distribution for the charmed-quark to fragment into a charmed hadron of type $h(= D^0, D^+, D_s^+, \Lambda_c^+)$ carrying a fraction z of the quark longitudinal momentum and transverse momentum p_T with respect to the quark direction. The number f_h is the mean multiplicity of the hadron h in neutrino charm-production. Analogously for anti-neutrinos, indicated by the barred quantities. Since only one c -quarks is produced in a CC interaction, one can set the normalization conditions as

$$\int_0^1 dz \int_0^\infty D_c^h(z, p_T^2) dp_T^2 = \int_0^1 dz \int_0^\infty \bar{D}_c^h(z, p_T^2) dp_T^2 = 1 \quad (3)$$

and

$$\sum_h f_h = \sum_h \bar{f}_h = 1.$$

The total cross-section for di-lepton charm-production, at a given energy, can then be written as

$$\sigma(\nu N \rightarrow \mu^- l^+ X)(E) = \sigma(\nu N \rightarrow \mu^- cX)(E) \times \sum_h f_h(E) \times BR_l^h$$

Energy (GeV)	f_{D^0}	f_{D^+}	$f_{D_s^+}$	$f_{\Lambda_c^+}$
5 – 20	0.32 ± 0.11	0.05 ± 0.06	0.18 ± 0.10	0.44 ± 0.12
20 – 40	0.50 ± 0.08	0.10 ± 0.08	0.22 ± 0.08	0.18 ± 0.07
40 – 80	0.64 ± 0.08	0.22 ± 0.09	0.09 ± 0.08	0.05 ± 0.04
> 80	0.60 ± 0.11	0.30 ± 0.11	0.00 ± 0.06	0.09 ± 0.08

Table 8: E531 prediction fraction results as obtained in Ref. [14].

$$= \sigma(\nu N \rightarrow \mu^- CX)(E) \times \overline{BR}_l(E) \quad (4)$$

where BR_l^h is the semi-leptonic branching fraction for the charmed hadron h .

From the previous formulae it is clear that in order to go from the di-lepton charm-production to the inclusive charm-production, BR_l^h and $f_h(E)$ should be known. The semi-leptonic branching fractions are measured with an accuracy of about 10% [15], while the $f_h(E)$'s have been measured directly only in one experiment, E531. However, a bias was found in the way E531 extracted $f_h(E)$. A detailed discussion on the re-fitting of these data with the bias removed is reported in Ref. [14]. For our purposes the measured energy dependence of f_h is relevant, see Table 8. The error on $\overline{BR}_l(E)$ has been computed as :

$$(\Delta \overline{BR}_l(E))^2 = \sum_i f_i^2(E) \cdot (\Delta BR_i)^2 + \sum_i BR_i^2 \cdot (\Delta f_i(E))^2 + 2 \cdot \sum_{j>i} BR_i \cdot BR_j \cdot cov_{j,i}(E)$$

where $cov_{j,i}(E)$ is the covariance matrix of the f_h values, defined as

$$cov_{i,j}(E) = \Delta f_i(E) \cdot \Delta f_j(E) \cdot cor_{i,j}(E)$$

and $cor_{i,j}(E)$ is the correlation among the f_h [14].

The average inclusive neutrino charm-production cross-section, normalized to the CC cross-section, as a function of the neutrino energy is shown in Table 9 and Fig. 3.

4.2 The world average total charm-production cross-section

The inclusive charm-production cross-section as measured in the E531 experiment and as derived from di-lepton data are shown in Fig. 3. The agreement between the two determinations is quite good, although the statistical errors are large. A better determination of the charmed fractions in the CHORUS experiment would reduce significantly the errors on the cross-section as derived from di-lepton data.

In order to parametrise the inclusive charm-production cross-section as a function of the energy, we have performed a fit with a polynomial function ($f(x)$) requiring that the constant term is zero:

Energy (GeV)	σ_C/σ_{CC} (%)	Energy (GeV)	σ_C/σ_{CC} (%)	Energy (GeV)	σ_C/σ_{CC} (%)
5	$3.12^{+1.01}_{-0.71}$	145	8.00 ± 1.63	285	9.05 ± 2.00
15	$3.75^{+0.99}_{-0.72}$	155	7.68 ± 1.62	295	9.05 ± 2.00
25	$5.53^{+1.46}_{-1.34}$	165	7.79 ± 1.64	350	9.68 ± 1.98
35	$3.82^{+1.20}_{-1.16}$	175	7.79 ± 1.64	450	10.11 ± 2.09
45	5.67 ± 1.06	185	8.63 ± 1.75	550	11.58 ± 2.99
55	5.44 ± 1.12	195	8.11 ± 1.70		
65	5.89 ± 1.19	205	8.84 ± 1.85		
75	6.78 ± 1.25	215	8.84 ± 1.85		
85	6.32 ± 1.37	225	8.95 ± 1.82		
95	6.74 ± 1.38	235	8.53 ± 1.82		
105	6.95 ± 1.57	245	8.84 ± 1.92		
115	6.84 ± 1.40	255	9.05 ± 2.00		
125	7.58 ± 1.73	265	9.05 ± 2.00		
135	7.58 ± 1.73	275	9.58 ± 1.94		

Table 9: Average inclusive neutrino charm-production cross-section, normalized to the CC cross-section, as a function of the neutrino energy.

$a_i \pm \Delta a_i$		a_1	a_2	a_3	a_4	a_5	a_6
0.23 ± 0.03	a_1	1.000	-0.828	0.266	0.228	0.028	-0.204
$-(0.31 \pm 0.03) \times 10^{-2}$	a_2	-0.828	1.000	-0.664	-0.132	0.096	0.196
$(0.21 \pm 0.07) \times 10^{-4}$	a_3	0.266	-0.664	1.000	-0.463	-0.168	0.151
$-(0.71 \pm 0.02) \times 10^{-7}$	a_4	0.228	-0.132	-0.463	1.000	-0.371	-0.225
$(0.115 \pm 0.003) \times 10^{-9}$	a_5	0.028	0.096	-0.168	-0.371	1.000	-0.735
$-(0.71 \pm 0.05) \times 10^{-13}$	a_6	-0.204	0.196	0.151	-0.225	-0.735	1.000

Table 10: Fitted parameters a_i together with the correlation coefficients $cor(a_i, a_j)$.

$$f(x) = a_1x + a_2x^2 + a_3x^3 + \dots + a_nx^n$$

Starting from $n = 6$, the χ^2 of the fit is very good, $P(\chi^2) > 0.99$, and mildly dependent on n . Therefore, we have chosen the smallest power for n . We have studied the effect of the different parametrisations on the prediction of the inclusive charm-production cross-section and we have found results different of at most 5% from the ones obtained with $n = 6$. Therefore, we have assigned to each prediction a systematical error of 5%. The fitted parameters a_i together with the correlation coefficients $cor(a_i, a_j)$ are given in Table 10. The fitted function is also shown in Fig. 3. Notice that the present parametrisation holds in the range $[0 \div 300]$ GeV.

As an application of our fit to the available data, we compute the expected D^0 production, normalised to the neutrino CC cross-section, in the CHORUS

experiment, whose neutrino beam has an average energy of 27 GeV. By convoluting the neutrino spectrum with the cross-section shown in Fig. 3, the expected average inclusive charm-production, normalized to the neutrino CC cross-section, is $(4.81 \pm 0.16 |_{stat} \pm 0.24 |_{syst})\%$, while the expected $\sigma(D^0)/\sigma_{CC}$ is $(2.58 \pm 0.26 |_{stat} \pm 0.13 |_{syst})\%$. This has to be compared with the measured value of $2.34 \pm 0.15 \pm 0.17\%$ [16]. Notice that the former experiment E531, with an average neutrino energy of about 22 GeV, measured the ratio $\sigma(D^0)/\sigma_{CC} = 2.19^{+0.39}_{-0.35}$ [17].

5 Conclusion

Over the past 30 years, several experiments have accumulated data on the (anti-)neutrino induced single-charm production with different techniques: opposite-sign dimuons have been used by calorimetric experiments, di-leptons (μ , e) by bubble chambers while only nuclear emulsion experiments have identified the charm through the visual observation of its decay. By combining all these data, a wide energy range (0-600 GeV) has been spanned, providing a good sensitivity to the threshold behavior of the cross-section.

We have presented a statistical way of combining all the available data and hence the extraction of the world averaged single-charm production cross-section as a function of the neutrino energy. A comparison of the D^0 production cross-section, normalised to the neutrino CC cross-section, with the result recently presented by the CHORUS Collaboration shows a good agreement.

Acknowledgment

We gratefully acknowledge U. Dore for useful discussions.

References

- [1] A. Benvenuti et al., Phys. Rev. Lett. 34 (1975) 419.
- [2] Abramowicz et al., Z. Phys. C 15 (1982) 19.
- [3] Ballagh et al., Phys. Rev. D 24 (1981) 7.
- [4] Columbia-Brookhaven National Laboratory (CBNL) Collaboration: data taken from Figure 1 of R. Brock, Phys. Rev. Lett. 44 (1980) 1027.
- [5] Astier et al., Phys. Lett. B 486 (2000) 35.
- [6] Rabinowitz et al., Phys. Rev. Lett. 70 (1993) 134.
- [7] Armenise et al., Phys. Lett. B 86 (1979) 115.
- [8] Haatuft et al., Nucl. Phys. B 222 (1983) 365.

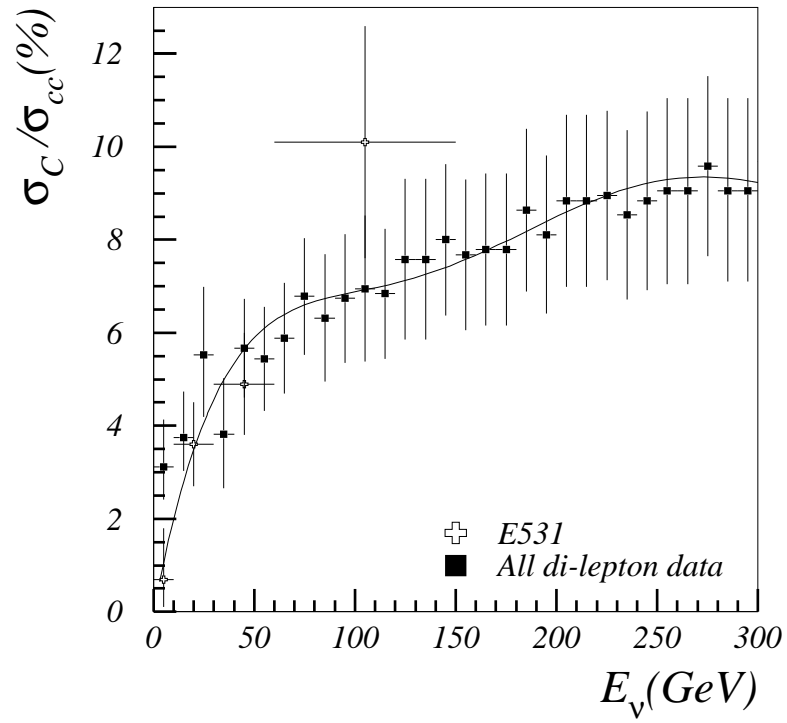


Figure 3: Average inclusive neutrino charm-production cross-section, normalized to the CC cross-section, as a function of the neutrino energy. The continuous line shows the result of a fit to the data with a polynomial function.

- [9] Baker et al., Phys. Rev. D 32 (1985) 531.
- [10] Foudas et al., Phys. Rev. Lett. 64 (1990) 1207.
- [11] Lang et al., Z. Phys. C 33 (1987) 483.
- [12] Ushida et al., Phys. Lett. B 206 (1988) 375.
- [13] E. Eskut et al., Nucl. Instr. Meth. A 401 (1997) 7.
- [14] T. Bolton, *hep-ex/9708014*.
- [15] Particle Data Group, Euro. J. 15 (2000) 1.
- [16] M. Guler for the CHORUS Collaboration, talk given at Europhysics Conference on HEP, Budapest, Hungary, 12-18 July 2001.
- [17] S.G. Frederiksen, Ph.D. Thesis, University of Ottawa (1987).

